The Structure of Idealized Upper-Tropospheric Shear Lines

MARTIN JUCKES

Meteorologisches Institut der Universität München, Munich, Germany

(Manuscript received 2 April 1998, in final form 17 November 1998)

ABSTRACT

The structure of idealized two-dimensional shear lines has been calculated for specified tropopause potential temperature anomalies. A cold anomaly corresponds to an intrusion of stratospheric air into the troposphere. A balanced hydrostatic primitive equation structure is derived using an iterative technique. The resulting wind and vertical displacement of the tropopause are compared with a recent result extending quasigeostrophic theory to situations where the variation of potential vorticity along an isentrope or isobar is large, as is the case, for instance, when the isosurface intersects the tropopause. The formulation of the theory is clarified by analyzing the relation between quasigeostrophic potential vorticity and Ertel's potential vorticity. The comparison between the low–Rossby number theoretical approximation and primitive equation structures confirms the theoretical prediction that the relative error is proportional to the Rossby number. The constant of proportionality is close to unity. The effect of the lower boundary condition on the shear line structure is analyzed. For a shear line consisting of an upper-tropospheric potential vorticity anomaly in the absence of a surface temperature anomaly it is found that the horizontal extent of the wind is not limited, as might have been expected, by the Rossby deformation radius, but rather by the largest scale of the shear line, which may be somewhat greater.

1. Introduction

The stratospheric and tropospheric air masses in midlatitudes can be characterized by a range of properties that change abruptly at or near the tropopause. These changes are mostly related, in varying degrees, to the fact that the troposphere experiences strong mixing in the vertical while the stratosphere is dominated by stable vertical entropy stratification. The contrast in entropy stratification forms the basis of the thermal definition of the tropopause. This definition is expressed in terms of the lapse rate of temperature with height. An alternative definition based on Ertel's potential vorticity P arose out of the work of Reed (1955) and Danielsen (1968) on tropopause folds. They documented stratospheric air being folded into the troposphere in a way that could not be described with the thermal definition. The fact that P is materially conserved under the conditions thought to be relevant for the formation of such folds implies that it can be used to trace the progress of the stratospheric air intruding into the troposphere. The tropopause defined in terms of P is known as the ''dynamical tropopause.''

Ertel's potential vorticity not only characterizes air masses but also provides an indication of how they will interact (Kleinschmidt 1950; Hoskins et al. 1985, hereafter HMR). In particular, the isentropic gradient of potential vorticity is related to the wind fields. For flows with low Rossby number the last point can be quantified through the quasigeostrophic potential vorticity q, whose isobaric gradient is, to leading order in Rossby number, proportional to the isentropic gradient of Ertel's potential vorticity (Charney and Stern 1962). From this it follows that the isobaric anomalies in q are related to the isentropic anomalies in Ertel's potential vorticity. This point is discussed further in section 2.

This study is concerned with cyclonic potential vorticity anomalies in the upper troposphere associated with a downward displacement of the tropopause. Such anomalies tend to congregate into two classes: shear lines and vortices. This is a consequence of the tendency of quasi-two-dimensional vortex flow to organize itself into coherent vortices. The exception occurs when a larger-scale strain flow overwhelms the inherent tendency of a vorticity anomaly to wrap up into a circular structure and instead stretches it out to form an elongated structure in which the vorticity is expressed in transverse shear: hence, a shear line.

The general problem of describing the evolution of the tropopause can be split into two stages: first, the diagnostic inversion stage (see HMR), in which wind and temperature fields are derived from a prescribed P field; and second, the dynamical step in which the P field is rearranged by advection. This study concentrates on the first stage. Comparison will be made between

Corresponding author address: Dr. Martin Juckes, Department of Atmospheric, Oceanic, and Planetary Physics, Clarendon Laboratory, Parks Road, Oxford OX1 3PU, United Kingdom.
E-mail: juckes@atm.ox.ac.uk

balanced solutions of the primitive equations and analytic low–Rossby number theory of Juckes (1994). This theory (referred to there as ''quasigeostrophic dynamics of the tropopause,'' hereafter QGT) is an extension of standard quasigeostrophic theory to take the sharp change in static stability at the tropopause into account. Unlike semigeostrophic theory, however, it only includes terms linear in Rossby number.

The anomalies relevant to the present study are formed when high-latitude stratospheric air is advected equatorward and downward into the troposphere. Holopainen and Rontu (1981) made a survey of such events occuring over western Europe. The phenomenon covers a range of scales from synoptic troughs, having strong interactions with the surface, to small-scale filamentary structures that cannot be resolved by the standard observational network but are revealed, for instance, in observations of water vapor in the upper troposphere (Appenzeller and Davies 1992; Browning 1993; Appenzeller et al. 1996; Wirth et al. 1998). The formation may be visualized in terms of the advection of potential vorticity anomalies along isentropes that descend from the polar stratosphere into midlatitudes. During this process the isentropes are not fixed surfaces; they move vertically so as to maintain a balance between the wind and thermal structures. To obtain the magnitude and structure of this vertical motion one must consider the three-dimensional structure of the anomaly.

The tropopause dynamics model of Juckes (1994, hereafter J94) offers an alternative approach. The work takes advantage of the fact that isentropic gradients of Ertel's potential vorticity (P) are weak both within the stratosphere and within the troposphere compared with the contrast that occurs across the tropopause. This means that a significant part of the structure is defined simply by the position of the tropopause. The climatological tropopause slopes downward to the poles and has a strong meridional potential temperature gradient. As polar air in the upper troposphere is advected equatorward, a region of anomalously cold tropopause potential temperatures is created. As with the isentropes, the tropopause is not a fixed surface during this process but moves vertically to maintain balance between wind and thermal structures. In J94 this situation is idealized by assuming that the isobaric gradient of q, proportional to the isentropic gradient of P in the small–Rossby number limit, vanishes identically except where isentropes intersect the tropopause. The theory then predicts, for a given tropopause potential temperature distribution, the geostrophic streamfunction and the vertical displacement of the tropopause δz_a. The subscript ''a'' is added here to emphasize that the vertical displacement of the tropopause takes place through ageostrophic advection in this model. That is, since the Rossby number expansion used here is based in pressure coordinates, the leading-order wind is taken to be purely isobaric. A different partition between first and second order is obtained if the expansion is carried out in isentropic coordinates. This theory is valid at small Rossby number, in which regime the slope of the tropopause is small. That is, the theory may apply, according to scale analysis, to vertical displacements of the tropopause of a few kilometers on the synoptic scales and a few hundred meters on the mesoscale. The scale analysis cannot, however, tell us precisely how the errors increase with Rossby number nor in what manner the true solution departs from the structure of the small–Rossby number limit. These questions will be addressed below.

Similar structures have been studied by Hoskins and Bretherton (1972) using semigeostrophic theory. The advantage of the approach used by J94 is that the vertical structure can be handled analytically. Applying the full semigeostrophic approach to a three-dimensional flow with a mobile tropopause is scarcely less demanding than solving the full primitive equations. With the approximate solution introduced by J94, on the other hand, a wide range of phenomena can be modeled very efficiently. For instance, Juckes (1995) derived an analytic solution for linear normal mode shear instability growing on the type of shear lines under discussion. Bayramli and Juckes (1998), using a linear, hydrostatic, primitive equation model, have shown that the analytic solution provides a reasonable description of the linear instability, even when the Rossby number is of order unity. A major difficulty in that study was the construction of basic states with which to initialize the primitive equation model. This work addresses the issue in detail, with the help of an algorithm for deriving primitive equation flows with vanishing isentropic gradients in potential vorticity.

If quasigeostrophic theory is used without modification in the vicinity of the tropopause, the potential temperature anomaly has a nonphysical discontinuity across the tropopause (e.g., Thorpe and Bishop 1995). J94 shows how to overcome this problem. There are two novel features here. First, rather than requiring that the quasigeostrophic potential vorticity be bounded, which gives a condition that $N^{-2}\psi_z$ should be continuous, it is proposed that the quasigeostrophic potential vorticity is not defined at the tropopause and that the boundary condition be given by the continuity of potential temperature. A second difference is that Thorpe and Bishop make no allowance for displacements of the tropopause. It is shown in J94 that, at small Rossby number, these displacements vary linearly with Rossby number. It is therefore appropriate to include them in a first-order theory. The results below confirm that the tropopause displacements induced by a potential temperature anomaly do indeed vary linearly with Rossby number at low Rossby number and that the amplitude of these displacements is given correctly by the theory of J94.

2. On quasigeostrophic and Ertel's potential vorticity

''Potential vorticity'' generally refers to a vorticity-like scalar quantity adjusted for changes in static sta-

bility so as to be conserved in adiabtaic motion. The forms relevant for the primitive equation and quasigeostrophic systems are, respectively, Ertel's potential vorticity P and the quasigeostrophic potential vorticity q. Both HMR and Vallis (1996) have emphasized the distinction between the two. It will be shown below, however, that there is a close connection if a rescaling of P is allowed for.

The relation between Ertel's potential vorticity and the quasigeostrophic counterpart has been obtained by Sadourny (1985) and Berrisford et al. (1993), using an isentropic coordinate approach. The derivation below is carried out in pressure coordinates, which serves to emphasize the distinction between the approximation that leads to the quasigeostrophic result and a naive expansion in Rossby number (Ro).

Ertel's potential vorticity is given by

$$P = \frac{(\boldsymbol{\zeta} + 2\boldsymbol{\Omega}) \cdot \boldsymbol{\nabla}\theta}{\rho}, \tag{1}$$

where $\boldsymbol{\zeta}$ is the vorticity, $\boldsymbol{\Omega}$ the planetary rotation, θ the potential temperature, and ρ the density.

The following discussion applies to hydrostatic flow. A log pressure vertical coordinate will be used:

$$z = -H_{00} \ln(p/p_{00}),$$

where

$$H_{00} = \frac{RT_{00}}{g}$$

is a characteristic scale height, $R = 287$ J K^{-1} kg^{-1} is the gas constant, $g = 10$ m s^{-2} is the acceleration due to gravity, and p is pressure. A subscript ''00'' will be used to indicate quantities that are characteristic for the atmosphere and a subscript ''sr'' for a static reference atmosphere. The flows considered below will be characterized by a mean surface temperature $T_{00} = 300$ K and a mean surface pressure $p_{00} = 10^5$ Pa. These values give $H_{00} = 8610$ m.

The vertical derivatives in the definition of Ertel's potential vorticity must be transformed using the following identity:

$$\frac{1}{\rho}\frac{\partial}{\partial z_{\text{geom}}} = \frac{1}{\rho_0}\frac{\partial}{\partial z},$$

where z_{geom} is the geometric height and $\rho_0 = p_{00}(RT_{00})^{-1} \exp[-z/H_{00}]$ is the pseudodensity for the log pressure coordinate system.

The connection between P and the quasigeostrophic potential vorticity q can be derived by first rescaling P to remove the exponential increase with height: let

$$P\dagger = \frac{P}{S_{\text{sr}}(\theta)}, \tag{2}$$

where

$$S_{\text{sr}}(\theta) = -g\left(\frac{d\theta_{\text{sr}}}{dp}\right)_{\theta_{\text{sr}}=\theta}$$

is related to the stability in a static reference state $\theta_{\text{sr}}(p)$. Thorpe and Bishop (1995) use a similar procedure but rescale the potential vorticity anomaly with a factor $[\rho_{\text{sr}}(z)P_{\text{sr}}(z)]^{-1}$. Vallis (1996) uses an approximate potential vorticity obtained without any rescaling. Both procedures have the disadvantage that the resulting quantities are not materially conserved in conditions when $P\dagger$ is conserved. That is, for adiabatic flow with $DS_{\text{sr}}/Dt = (dS_{\text{sr}}/d\theta)(D\theta/Dt) = 0$ it follows that $DP\dagger/Dt = 0$, where $D/Dt = \partial/\partial t + \mathbf{u} \cdot \boldsymbol{\nabla}$ is the material derivative.

In small–Rossby number flow we have

$$\begin{aligned} P\dagger &\approx f\frac{\partial\theta}{\partial p}\left(\frac{d\theta_{\text{sr}}}{dp}\right)^{-1} + \zeta, \\ &= f\left(1 + \left(\frac{\partial\theta}{\partial p}\right)'^{\theta}\left(\frac{d\theta_{\text{sr}}}{dp}\right)^{-1}\right) + \zeta, \end{aligned} \tag{3}$$

where the product of the relative vorticity and the anomaly in static stability has been neglected as being $O(\text{Ro}^2)$, as have terms related to the horizontal components of $\boldsymbol{\zeta}$. The terms containing the horizontal components of $\boldsymbol{\Omega}$ are smaller than that containing the vertical component by a factor $z_{\text{sc}}/x_{\text{sc}}$. This is generally of the same order of magnitude as Ro^2 for low Ro midlatitude flows. The superscript ''$'^{\theta}$'' indicates an isentropic anomaly, that is, an anomaly relative to the static reference value at the same potential temperature. Similarly, ''$'^{p}$'' will indicate an isobaric anomaly. The anomaly in static stability $(\partial\theta/\partial p)'^{\theta}$ can be split into two terms: one arising from the isobaric anomaly in potential temperature, θ'^{p}; and one arising from the difference between the reference state at the current pressure level and that at the current isentrope. Consider a point A with potential temperature θ_A and pressure p_A:

$$\begin{aligned} \left(\frac{\partial\theta}{\partial p}\right)'^{\theta}_{p=p_A} &\equiv \frac{\partial\theta}{\partial p} - \frac{d\theta_{\text{sr}}}{dp} \\ &= \frac{\partial\theta'^{p}}{\partial p} + \left(\left.\frac{d\theta_{\text{sr}}}{dp}\right|_{p=p_A} - \left.\frac{d\theta_{\text{sr}}}{dp}\right|_{p=p_A-p'^{\theta}}\right), \end{aligned} \tag{4}$$

where p'^{θ} is the pressure anomaly of the isentropic surface. That is, $p = p_A - p'^{\theta}$ is the pressure level of the isentrope θ_A in the reference state. This pressure anomaly is related to the potential temperature anomaly of the isobaric surface by

$$\theta'^{p} = -\frac{d\theta_{\text{sr}}}{dp}p'^{\theta}, \tag{5}$$

provided the anomalies are sufficiently small [this follows from $\theta_{\text{sr}}(p_A - p'^{\theta}) = \theta_A$ and $\theta_{\text{sr}}(p_A) + \theta'^{p} = \theta_A$]. Approximating the second term in (4) with the first term

in its Taylor expansion and substituting for p'^{θ} from (5) gives

$$\frac{\partial\theta}{\partial p} - \frac{d\theta_{\rm sr}}{dp} = \frac{\partial\theta'^{p}}{\partial p} - \frac{d^2\theta_{\rm sr}}{dp^2}\left(\frac{d\theta_{\rm sr}}{dp}\right)^{-1}\theta'^{p} = \frac{d\theta_{\rm sr}}{dp}\frac{\partial}{\partial p}\left[\left(\frac{d\theta_{\rm sr}}{dp}\right)^{-1}\theta'^{p}\right]. \quad (6)$$

The usual expression for q is obtained when (6) is substituted into (3) and the following standard definitions are used:

$$(u_g,\ v_g,\ \theta'^{p}) = \left(-\psi_y,\ \psi_x,\ \frac{f_0\theta_{\rm sr}}{g}\psi_z\right), \quad (7)$$

$$\frac{\partial}{\partial p} = -\frac{1}{g\rho_0}\frac{\partial}{\partial z} \quad \text{and}$$

$$N^2 = \frac{g}{\theta_{\rm sr}}\frac{d\theta_{\rm sr}}{dz} = -\frac{g^2\rho_0}{\theta_{\rm sr}}\frac{d\theta_{\rm sr}}{dp}, \quad (8)$$

giving

$$P\dagger \approx f + \psi_{xx} + \psi_{yy} + \frac{f_0^2}{\rho_0}\frac{\partial}{\partial z}\left(\frac{\rho_0}{N^2}\frac{\partial\psi}{\partial z}\right) \equiv q, \quad (9)$$

where ψ is the geostrophic streamfunction, f the Coriolis parameter, f_0 the latter at a reference latitude, and N^2 the Brunt–Väisälä frequency of the log pressure formulation. Equation (7) includes what Charney and Stern (1962) refer to as the quasi-Boussinesq approximation, in which the scale height of the potential temperature is assumed to be much greater than the height scale of the flow.

Equation (9) shows that q is the leading-order approximation in Rossby number to $P\dagger$, Ertel's potential vorticity scaled with a materially conserved reference static stability. That is, it is the natural leading-order approximation when Ertel's potential vorticity is normalized to remove the exponential increase with height and when this is done in a way that respects the important property of material conservation.

From (9) it follows that

$$P \approx qS_{\rm sr}(\theta). \quad (10)$$

Although q is not a direct approximation to P, the relation between the two is straightforward.

The result is effectively a restatement of Charney and Stern's statement that

$$\nabla_p q \propto \nabla_\theta P,$$

where ∇_p and ∇_θ are isobaric and isentropic gradients, respectively. The derivation here is slightly more direct in that it deals directly with the anomalies rather than with gradients. This emphasizes the kinematic nature of the identity.

The ''sr'' reference atmosphere may be a horizontal average of an observed atmosphere, but it could also be an idealization. The only restriction is that the departure of the actual atmosphere from the reference should not be significantly greater than the horizontal variability within the atmosphere. In the theory of J94 the stratosphere and troposphere are treated separately. In this case it is the departure from the reference profile of the relevant domain and the corresponding horizontal variability that are relevant.

For stratospheric applications an isothermal reference state may be acceptable. This would give

$$S_{\rm sr}^{\rm it} = \frac{g\kappa}{p_{00}}\frac{\theta^{1+1/\kappa}}{T_{00}^{1/\kappa}}$$

and

$$P\dagger^{\rm it} = \frac{p_{00}T_{00}^{1/\kappa}}{g\kappa}\frac{(\boldsymbol{\zeta} + 2\boldsymbol{\Omega})\cdot\nabla\theta}{\rho\theta^{1+1/\kappa}},$$

where $\kappa = R/c_p$, with c_p the specific heat capacity at constant pressure. This form of potential vorticity is equivalent to that proposed by Lait (1994), where the advantages of a rescaled potential vorticity for the presentation and interpretation of stratospheric data are discussed.

For tropospheric application the isothermal reference atmosphere is not acceptable, but a constant N^2 atmosphere provides a reasonable basis (remembering that N^2 is here defined through log pressure coordinate and so differs slightly from the true Brunt–Väisälä frequency). The resulting reference profile has $\theta = \theta_{00}\exp(zN^2/g)$ and stability

$$S_{\rm sr}^{N} = \frac{N^2\theta_{00}}{\rho_{00}g}\left(\frac{\theta}{\theta_{00}}\right)^{1+(g/N^2H_{00})},$$

where $\rho_{00} = \rho_0(0)$ is the surface pseudo density. The corresponding potential vorticity is

$$P^N = \frac{\rho_{00}g}{N^2\theta_{00}}\frac{(\boldsymbol{\zeta} + 2\boldsymbol{\Omega})\cdot\nabla\theta}{\rho}\left(\frac{\theta_{00}}{\theta}\right)^{1+(g/N^2H_{00})}.$$

As for Ertel's potential vorticity, this quantity is materially conserved for frictionless adiabatic flow. It has the advantage that it reduces to the quasigeostrophic potential vorticity in the low–Rossby number limit. It is determined by local quantities apart from the constants ρ_{00}, θ_{00}, H_{00}, N^2, and g, which define the reference atmosphere.

These results illustrate the theoretical link between the quasigeostrophic potential vorticity and forms relevant to the primitive equations. In practice the complex form of P^N may outweigh the advantage brought by its closer relation to q, but the important point is that there is no fundamental distinction between potential vorticity in the quasigeostrophic system and that in the primitive equation system.

This derivation clarifies the nature of the approximations leading to (9). At the tropopause the approximations (5) and (6) become invalid. The potential vor-

ticity equation [(9)] is only valid within the troposphere and within the stratosphere, but not along the boundary between. It follows that the solution of (9) requires not only external boundary conditions but also internal boundary conditions linking the tropospheric and stratospheric solutions. In J94 it is shown that the physically necessary condtions, continuity of ψ and θ across the tropopause, are also sufficient to determine the solution.

3. Equations and numerical techniques

This study is concerned with steady flows that are independent of x. The starting point will be the primitive equations in log pressure coordinates. Isentropic coordinates offer some advantages, but this work was started with the idea of using the shear lines as initial flows for stability studies in a pressure-based three-dimensional primitive equation model. It is therefore desirable to have the flow variables in the latter coordinate system.

The equations are solved in physical space rather than taking advantage of the geostrophic coordinate transformation that, for the constant f problem considered here, would simplify the problem somewhat. This is partly to obtain variables on a grid suitable for a three-dimensional primitive equation model and partly to allow for possible generalization to the variable f case. The equations can be solved to machine accuracy in physical coordinates, so this choice of coordinates does not affect the results.

The potential temperature, temperature, density, and geopotential height of the static atmosphere (θ_{sr}, T_{sr}, ρ_{sr}, and Φ_{sr}, respectively) satisfy

$$\theta_{sr} = T_{sr}e^{\kappa z/H_{00}}, \tag{11a}$$

$$p_{00}e^{-z/H_{00}} = R\rho_{sr}T_{sr}, \tag{11b}$$

$$\frac{d\Phi_{sr}}{dz} = \frac{gT_{sr}}{T_{00}}. \tag{11c}$$

The actual static reference profile used will be prescribed in terms of the functional relationship between potential vorticity and potential temperature, discussed in more detail below.

After setting v, $w = 0$ and $\partial/\partial t \equiv \partial/\partial x \equiv 0$, the primitive equations for two-dimensional flow geometry with log pressure as a vertical coordinate are

$$fu + \Phi_y = 0, \tag{12a}$$

$$\Phi_z = \frac{gT}{T_{00}} \tag{12b}$$

(e.g., Andrews et al. 1987, p. 118).

The potential vorticity takes the form

$$P(y, z) = [(f^2 + \Phi_{yy})(\Phi_{zz} + \kappa H_{00}^{-1}\Phi_z) - \Phi_{yz}^2] \times \frac{T_{00}}{gf\rho_0(z)} \exp\left(\frac{\kappa z}{H_{00}}\right) \equiv \mathcal{N}(\Phi). \tag{13}$$

For a given potential vorticity field $P(y, z)$ associated with a displaced tropopause the nonlinear partial differential equation (13) must be solved to find Φ. This is done with an iterative method. Suppose $\Phi^{(n)}$ is an approximate solution. A correction $\phi^{(n)}$ is found by linearizing the difference $\mathcal{N}[\Phi^{(n)} + \phi^{(n)}] - \mathcal{N}[\Phi^{(n)}]$. This gives

$$[f^2 + \Phi_{yy}^{(n)}][\phi_{zz}^{(n)} + \kappa H_{00}^{-1}\phi_z^{(n)}] + [\Phi_{zz}^{(n)} + \kappa H_{00}^{-1}\Phi_z^{(n)}]\phi_{yy}^{(n)} - 2\Phi_{yz}^{(n)}\phi_{yz}^{(n)} = \frac{gf\rho_0}{T_{00}}\{P - \mathcal{N}[\Phi^{(n)}]\}. \tag{14}$$

This linear equation is elliptic provided $f\mathcal{N}[\Phi^{(n)}] > 0$. Following Wirth (1995), (14) can be solved iteratively using the routine D03EDF from the Numerical Algorithms Group. There are now two iterative loops, one to solve (14) and a second using successive solutions of (14) to approach a solution of (13). The double iteration is potentially expensive, but it is found, following Salby and Juckes (1994), that an approximate solution of the elliptic equation is sufficient to obtain an improved estimate of the Φ. Suppose $\phi^{(n,1)}$ is the approximate solution to (14) obtained after one iteration of D03EDF. We take $\Phi^{(n+1)} = \Phi^{(n)} + c_d\phi^{(n,1)} + c_0 + c_1 \exp(-\kappa z/H_{00})$, where c_0 and c_1 are constants of integration. Once the approximate solution of (14) is found, c_0 and c_1 are chosen to maintain the lower boundary condition on either $\overline{\Phi}$ or $d\overline{\Phi}/dz$ and to satisfy $\overline{\theta}(H_{tp}) = 324$ K, where H_{tp} is the undisturbed height of the tropopause and $\overline{(\,)}$ denotes an average over y. The iteration is continued until the residual $P - \mathcal{N}[\Phi^{(n)}]$ is sufficiently small. The damping factor c_d is chosen to ensure stability of the iteration. A value of 0.4 ensures convergence for the cases discussed below. If a larger value is used, there is a risk that $f\mathcal{N}[\Phi^{(n)}]$ can become negative at some iteration, n. This makes the linear equation [(14)] nonelliptic and causes the iteration procedure to diverge.

The primitive equation equivalent of uniform q within each air mass, prescribed in J94, is zero isentropic gradients of P in each air mass. In other words, the values of P within the stratosphere or within the troposphere are determined by functions of potential temperature, $\mathcal{P}_s$ and $\mathcal{P}_t$, respectively. These functions are prescribed as follows:

$$\mathcal{P}_{s/t}[\theta] = \frac{f\Gamma_{s/t}}{\rho_{00}}\left(\frac{\theta}{\theta_{00}}\right)^{1+(g/N^2H_{00})}, \tag{15}$$

where $\Gamma_{s/t}$ is a characteristic lapse rate $d\theta/dz$ for the stratosphere–troposphere. The corresponding potential temperature profiles, satisfying $\mathcal{P}_{s/t}(\theta) = f\rho^{-1}d\theta/dz$, are given by

$$\theta = \theta_{00} \exp\left[\frac{N_{s/t}^2 z}{g}\right].$$

The potential vorticity is specified as a linear com-

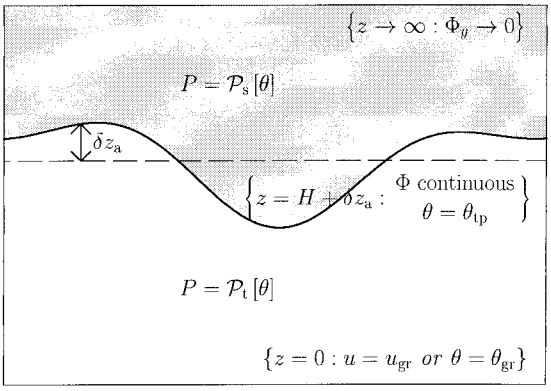

FIG. 1. The equations satisfied by the two-dimensional steady primitive equation flow. In addition, Eqs. (12a) and (12b) are satisfied throughout the domain. The shaded region is the stratosphere and the dashed line shows the undisturbed tropopause height $z = H_{tp}$.

bination of the stratospheric and tropospheric functions such as to give a smooth transition at the tropopause:

$$\mathcal{P}[\theta(y, z)] \equiv \mathcal{P}_t[\theta(y, z)] + \{\mathcal{P}_s[\theta(y, z)] - \mathcal{P}_t[\theta(y, z)]\} \times \mathcal{H}[\theta(y, z) - \theta_{tp}(y), \theta_{in}], \tag{16}$$

where

$$\mathcal{H}(s, r) = \frac{1}{2}\left[1 + \mathrm{erf}\left(\frac{s}{r}\right)\right],$$

"erf" being the error function. The function $\mathcal{H}(s, r)$ has value 0 at large negative s, unity at large positive s, and a transition centered on $s = 0$ with width r. The sharpness of the tropopause in the profile defined by (16) is thus given by θ_{in}. Since $\theta(y, z)$ is part of the solution and not known a priori, $P(y, z)$ must be updated at iteration n using the latest estimate $\theta^{(n-1)}(y, z)$. This is done as follows:

$$P^{(n)}(y, z) = (1 - c_d)P^{(n-1)}(y, z) + c_d\mathcal{P}[\theta^{(n-1)}(y, z)].$$

In Eq. (14) a term proportional to $d\mathcal{P}/d\theta$ has been neglected. Including this term tends to make the iteration scheme unstable.

It remains to define the horizontal structure $\theta_{tp}(y)$ appearing in (16). The smoothed step function $\mathcal{H}$ is used again as follows:

$$\theta_{tp}(y) = \Theta(y; y_{sl}, y_{in}, \theta_{sl}) \equiv \theta_{00} + \frac{\theta_{sl}}{2}[\mathcal{H}(y + y_{sl}, y_{in}) - \mathcal{H}(y - y_{sl}, y_{in})]. \tag{17}$$

This gives a strip of width $2y_{sl}$ and amplitude θ_{sl} bounded by fronts of width y_{in}.

When the tropopause is of finite thickness ($\theta_{in} > 0$) the function $\theta_{tp}(y)$ does not correspond exactly to the potential temperature of any one potential vorticity surface, but all surfaces within the tropopause have potential temperature distributions close to $\theta_{tp}(y)$, provided θ_{in} is sufficiently small.

The physical parameters of the undisturbed static atmosphere are the sharpness of the tropopause θ_{in} ("in" indicates an "internal" scale, in some sense); the potential temperature of the surface (θ_{00}) and of the tropopause θ_{tp}; the potential temperature lapse rates of stratosphere and troposphere Γ_s and Γ_t; and the density-scale height H_{00}. The shear line is then defined by the sharpness of the horizontal potential temperature gradients along the tropopause y_{in}, the half-width of the shear line y_{sl}, and the amplitude of the potential temperature anomaly θ_{sl}. Unless otherwise stated, the values used below are $\Gamma_s = 18$ K km^{-1}, $\Gamma_t = 3$ K km^{-1}, $\theta_{tp} = 324$ K, $\theta_{00} = 300$ K, and $\theta_{in} = 2$ K. These parameters, together with the functional relation (16) define the static reference atmosphere.

Numerical parameters are the size of the domain L_{dom} and H_{dom}, the number of grid points $N \times M$, and the error tolerance ϵ_{tol}. There is also the damping factor c_d, but this has no effect on the solution, provided convergence is achieved (no evidence of multiple solutions of the nonlinear equation has been found). A 256 horizontal by 512 vertical grid is used below, apart from one figure showing the effect of using lower resolution. The domain size is $L_{dom} = 3H_{00}N_t/f = 2400$ km and $H_{dom} = 18$ km, giving a grid spacing of about 35 m in the vertical and 10 km in the horizontal (the horizontal grid extends from $y = 0$ to L_{dom}; $y = 0$ is an axis of symmetry). Solutions will be presented using either constant potential temperature or constant geopotential as a lower boundary condition.

4. QGT theory

J94 gives expressions for the streamfunction and vertical displacement associated with given potential temperature anomalies on the tropopause and lower boundary. As explained in the introduction, this work is motivated by the fact that these potential temperature anomalies are conserved in adiabatic flow, so their evolution is given by conceptually straightforward rearrangement by the wind. The theory requires two idealizations: low Rossby number and weak isentropic gradients of potential vorticity both within the troposphere and within the stratosphere. It is the aim of this paper to look at the effects of relaxing the former idealization while retaining the latter. This section reviews the QGT theory and analyzes the structure relevant to shear lines in more detail.

Figure 2 shows a sketch of the envisaged flow. The quasigeostrophic potential vorticity anomaly vanishes both above and below the tropopause. At the tropopause the boundary conditions are continuity of the geostrophic streamfunction ψ and equality of both the stratospheric and tropospheric potential temperatures to the prescribed tropopause potential temperature. The unknown vertical displacement of the tropopause δz_a is

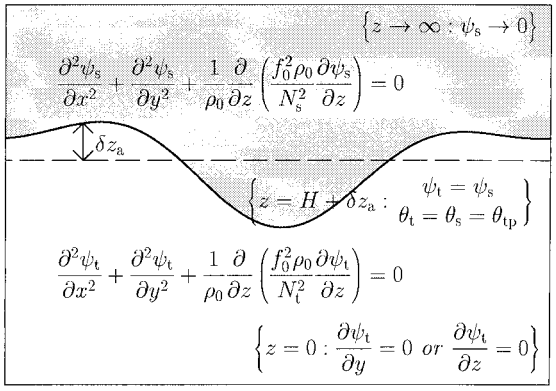

FIG. 2. The elliptical equations satisfied by ψ_s in the stratosphere (shaded) and by ψ_t in the troposphere are shown. The bracketed expressions show the boundary conditions used at the external boundaries $z = 0$, $z = \infty$, and at the internal boundary (the tropopause $z = H_{tp} + \delta z_a$. The dashed line shows the undisturbed tropopause height $z = H_{tp}$.

dealt with by applying approximate boundary conditions at the mean tropopause height, using

$$\theta_s|_{z=H_{tp}+\delta z_a} \approx \theta_s|_{z=H_{tp}} + \delta z_a\Gamma_s, \qquad \psi_s|_{z=H_{tp}+\delta z_a} \approx \psi_s|_{z=H_{tp}},$$

$$\theta_t|_{z=H_{tp}+\delta z_a} \approx \theta_t|_{z=H_{tp}} + \delta z_a\Gamma_t, \quad \text{and}$$

$$\psi_t|_{z=H_{tp}+\delta z_a} \approx \psi_t|_{z=H_{tp}}.$$

These approximations are correct to leading order in Rossby number; the product of δz_a and the static stability anomaly has been neglected as being of order Rossby number smaller. The problem now has one boundary condition at $z = 0$, one at $z \to \infty$, and three conditions at the tropopause. The usual complement for a second-order differential equation would only have two conditions at the tropopause, but here the extra condition is necessary and sufficient to determine an extra unknown: the vertical displacement of the tropopause.

The problem can then be solved by decomposing all the fields into horizontal Fourier coefficients. If the lower boundary potential temparature anomaly is set to zero the result takes the form

$$\tilde{\psi}_{tp}(k, l) = \frac{gH_{00}\tilde{G}_1^\theta}{f\theta_{00}}\tilde{\theta}_{tp}(k, l) \tag{18a}$$

$$\delta\tilde{z}_a(k, l) = \tilde{G}_2^\theta\tilde{\theta}_{tp}(k, l), \tag{18b}$$

where $\tilde{(\ )}$ indicates the coefficient of a horizontal Fourier transform (more details in J94) with horizontal wavenumber (k, l). At this stage there is no restriction on the horizontal structure beyond the requirement of small Rossby number. For the comparison with the primitive equations a two-dimensional flow will be generated by setting $k = 0$. Here $\tilde{G}_i^\theta$, $i = 1, 2$ are functions of total horizontal wavenumber $\lambda = \sqrt{k^2 + l^2}$ and also of Γ_t, Γ_s, H_{00}, and H_{tp}. The superscript indicates the form of the lower boundary condition: "θ" for Neumann boundary condition $\theta_{gr} = 0$ and "u" for Dirichlet boundary contition $u_{gr} = 0$ (the subscript "gr" indicates evaluation at $z = 0$).

The vertical wavenumbers corresponding to a given horizontal wavenumber are $(2H_{00})^{-1} \pm m_{s/t}$, where

$$m_{s/t} = \sqrt{\frac{1}{4H_{00}^2} + \frac{N_{s/t}^2\lambda^2}{f_0^2}}. \tag{19}$$

For convenience, we define $a = (2H_{00})^{-1} - m_s$, $b = (2H_{00})^{-1} - m_t$, and $c = (2H_{00})^{-1} + m_t$. J94 included terms representing the effects of finite-scale heights in potential temperature, these terms will be neglected here since they are only of significance for planetary-scale disturbances.

The coefficents relating the streamfunction and vertical displacement to the potential temperature anomaly, with a lower boundary condition of zero potential temperture anomaly, are (from J94)

$$\tilde{G}_1^\theta = -\frac{(\Gamma_s - \Gamma_t)}{H_{00}}(ce^{-m_tH_{tp}} - be^{m_tH_{tp}})/\mathcal{D}^\theta \tag{20a}$$

and

$$\tilde{G}_2^\theta = [b(c - a)e^{m_tH_{tp}} - c(b - a)e^{-m_tH_{tp}}]/\mathcal{D}^\theta, \tag{20b}$$

where

$$\mathcal{D}^\theta = (a\Gamma_t - b\Gamma_s)ce^{-m_tH_{tp}} - (a\Gamma_t - c\Gamma_s)be^{m_tH_{tp}}. \tag{20c}$$

Similar expressions are obtained if the lower boundary condition $\theta_{gr} = 0$ is replaced by $\psi_{gr} = 0$ [i.e., replace (5.9) of J94 with $Be^{m_tH_{tp}} + Ce^{-m_tH_{tp}} = 0$ in the notation of that paper]. The results are as (18) except that $\tilde{G}_i^\theta$ should be replaced with $\tilde{G}_i^u$ given by

$$\tilde{G}_1^u = -\frac{(\Gamma_s - \Gamma_t)}{H_{00}}(e^{-m_tH_{tp}} - e^{m_tH_{tp}})/\mathcal{D}^u \tag{21a}$$

and

$$\tilde{G}_2^u = [(c - a)e^{m_tH_{tp}} - (b - a)e^{-m_tH_{tp}}]/\mathcal{D}^u, \tag{21b}$$

where

$$\mathcal{D}^u = (a\Gamma_t - b\Gamma_s)e^{-m_tH_{tp}} - (a\Gamma_t - c\Gamma_s)e^{m_tH_{tp}}. \tag{21c}$$

These expressions depend on a large number of parameters, so two levels of approximation, obtained by eliminating parameters that are in some circumstances marginal, will also be discussed. The first is to form the Boussinesq approximation by taking the limit $1/H_{00} \to 0$. The neglected term is of the form $H_{tp}/(2H_{00})$, which has a value close to 0.5. It is in a certain sense inconsistent to neglect the scale height of density while retaining the interaction between the ground and tropopause. It is nevertheless a useful approximation because the finite density-scale height makes only qualitative changes to the flow structure. The neglect of the interaction between tropopause and ground, on the other hand, is a fundamental change to the system since it eliminates baroclinic modes and leaves a quasi-barotropic system. At the first level of approximation we

have $\tilde{G}_i^{\cdot|\text{Bous}}$, given by taking the limit $H_{00} \to \infty$ in (20) and (21). The constants a, b, c, and $m_{s/t}$ reduce to the following values:

$$a^{\text{Bous}} = -m_s^{\text{Bous}} = -N_s\lambda/f,$$
$$b^{\text{Bous}} = -m_t^{\text{Bous}} = -N_t\lambda/f,$$
$$c^{\text{Bous}} = m_t^{\text{Bous}} = N_t\lambda/f. \tag{22}$$

Substituting in Eqs. (20a)–(20c), which apply to the Neumann lower boundary condition, gives

$$\tilde{G}_1^{\theta|\text{Bous}} = \tilde{G}_1^{\min}\left(\frac{N_t + N_s}{N_t + N_s \tanh(N_t\lambda H_{\text{tp}}/f)}\right), \tag{23a}$$

$$\tilde{G}_2^{\theta|\text{Bous}} = \tilde{G}_2^{\min}\left(\frac{N_s + N_t \tanh(N_t\lambda H_{\text{tp}}/f)}{N_t + N_s \tanh(N_t\lambda H_{\text{tp}}/f)}\right), \tag{23b}$$

where the $\tilde{G}_{1,2}^{\min}$ (the ''minimal'' model) values correspond to the second level of approximation. This is obtained in the limit $\lambda H_{\text{tp}} \to \infty$ in (20) or (21) (this limit corresponds to neglecting the effect of the lower boundary on the tropopause):

$$\tilde{G}_1^{\min} = \frac{f(N_s - N_t)}{\lambda H_{00} N_s N_t}, \tag{24a}$$

$$\tilde{G}_2^{\min} = \frac{1}{\sqrt{\Gamma_s \Gamma_t}}. \tag{24b}$$

Similarly, for the Dirichlet boundary condition, substituting (22) in (21) gives

$$\tilde{G}_1^{u|\text{Bous}} = \tilde{G}_1^{\min}\left[\frac{N_t + N_s}{N_t + N_s \coth(N_t\lambda H_{\text{tp}}/f)}\right], \tag{25a}$$

$$\tilde{G}_2^{u|\text{Bous}} = \tilde{G}_2^{\min}\left[\frac{N_t + N_s \tanh(N_t\lambda H_{\text{tp}}/f)}{N_s + N_t \tanh(N_t\lambda H_{\text{tp}}/f)}\right]. \tag{25b}$$

The Dirichlet lower boundary condition (zero wind) reduces both δz_a and ψ relative to the minimal model. In the case of zero surface temperature anomaly the reverse effect is observed. This is a modification of the ''vacuum cleaner'' analogy, introduced by HMR, which refers to the way in which cyclonic potential vorticity anomalies draw up the isentropic surfaces below them. If there is a boundary, however, that prevents the isentropic surfaces from being displaced upward, the potential vorticity anomaly is, in the present case, displaced downward. It will be confirmed below that QGT gives the magnitude of this effect correctly to leading order in Rossby number.

For Boussinesq flow the effect of the lower boundary can be visualized as being equivalent to having a virtual potential vorticity anomaly, obtained by reflecting the actual anomaly in the boundary $z = 0$ (Bishop and Thorpe 1994). If the virtual anomaly is given the same sign as the actual anomaly, a ψ field is obtained that is symmetric about $z = 0$ and, hence, satisfies $\partial\psi/\partial z = 0$ at $z = 0$. If, on the other hand, the virtual anomaly has the opposite sign, the ψ field is antisymmetric in $z = 0$ and, hence, satifies $\psi = 0$ at $z = 0$. It follows that the $\partial\psi/\partial z = 0$ boundary condition tends to strengthen the anomaly whereas the $\psi = 0$ boundary condition tends to weaken it. For non-Boussinesq flow this image method no longer works, but the qualitative effect of the lower boundary remains the same.

The minimal model given by (24) has an attractive simplicity. As far as the evolution is concerned it is isomorphic to the dynamics of potential temperature anomalies on a solid surface bounding a semi-infinite fluid of uniform potential vorticity, which has been discussed by Blumen (1978) and Held et al. (1995). The temperature anomalies behave to a certain extent like vorticity anomalies in nondivergent two-dimensional flow: there is a tendency for variance to be transfered to small scales and energy to large scales. Strips of anomalous tropopause potential temperature wrap up into vortices in a process analogous to Rayleigh instability in nondivergent vortex dynamics. The simple relation between the vertical displacement of the tropopause and temperature anomalies in the upper troposphere implied by (24b) was used by Juckes (1997) to derive a relationship between the meridional heat flux in the troposphere and the mean meridional mass flux in the lower reaches of the stratosphere. Somewhat suprisingly the latter flux is directed away from the winter pole toward the Tropics. The results below will show that the QGT theory is accurate, at least in two-dimensional flow, for the Rossby number regime of the synoptic-scale waves that generate this mass flux.

Further insight into the structure described by Eqs. (20) and (21) can be obtained by studying the limits of large and small scales. These approximations are evaluated in the appendix. Figure 3a displays the results for the Dirichlet lower boundary condition. The long-wave limit only becomes accurate at $\lambda \leq 0.2$, while the large λ approximation works down to $\lambda = 1$. This short wave limit, however, does not include any information about the interaction of the surface and the tropopause. The problem is that this interaction, which is governed by scales of the order $N_t H_{\text{tp}}/f$, is exponentially small in the large wavenumber limit, so the asymptotic analysis of that limit is dominated by terms related to the scale height H_{00} that enter algebraically.

Figure 3b shows the corresponding physical space structure. This gives the structure of the horizontal wind on the tropopause u_{tp} that would be associated with an arbitrarily thin strip of anomalous potential temperature. The solid line is evaluated through a numerical fast Fourier transform. A grid with 16 384 points is used to ensure that there is enough resolution to resolve the small y behavior and a large enough range to capture the large y structure. The large y limit does not approach the true curve in the range plotted, but it is asymptotically correct at sufficiently large y. The problem is that the analysis picks out the largest horizontal length scale $N_s H_{00}/f$, and this has a relatively minor role. These re-

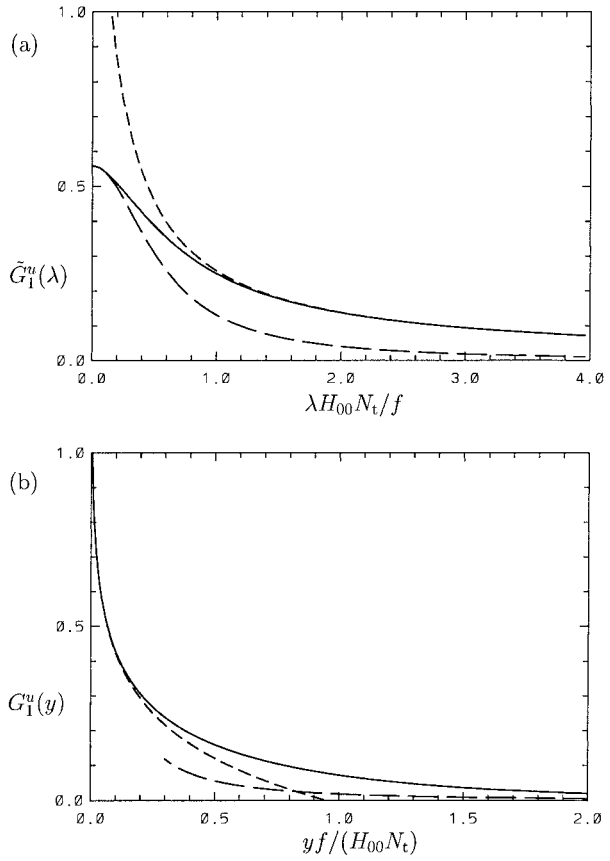

FIG. 3. The structure of the Green's function relating the quasigeostrophic streamfunction at the tropopause to the potential temperature of the tropopause with a lower boundary condition of zero wind. (a) In Fourier space: $\tilde{G}_1^u(\lambda)$ (solid line) against $\lambda = \sqrt{k^2 + l^2}$. The dashed lines show asymptotic approximations for the limits $\lambda \to 0$ and $\lambda \to \infty$ derived in the appendix. (b) In physical space: $G_1^u(y)$ (solid line) and the corresponding asymptotic approximations.

sults thus give a useful approximation for the small-scale structure but do not do so for scales in the range 0.5–2 Rossby radii.

The corresponding results for G_1^θ, described in the appendix, reveal an important property of the far-field flow: the response has unlimited horizontal extent, even in non-Boussinesq flow. If there were no lower boundary, on the other hand, the meridional extent would be limited by the Rossby radius based on twice the density-scale height. The unlimited extent here means that the numerical solutions will be affected by the meridional boundary conditions. It will be shown that this is indeed the case when the primitive equations are solved. The scale height of potential temperature has been neglected here, as has the difference between the potential temperature at $z = 0$ and that at $\Phi = 0$. These two effects are of similar order and would imply a horizontal scale of several thousand kilometers if the potential temperature scale height appropriate for the stratosphere is taken. This result applies to a shear line with infinite length in the x direction: in practice the length is, of course, finite. The implication is that the relevant scale for the extent of the region influenced by the anomaly is the length of the tropopause anomaly. Consequently, a streamer that is several deformation radii long and a few hundred kilometers wide may have a very large radius of influence. A shear line defined with the $u_{gr} = 0$ boundary condition, on the other hand, has a relatively small radius of influence. This can be viewed as being due to the cancellation between the fields due to a surface potential temperature anomaly and those due to the tropopause anomaly. If the two anomalies become decoupled, by differential advection, a strong surface wind field may be generated.

This property may be relevant to events described in a recent analysis of severe weather events in the Alps. It has been found (Massacand et al. 1998) that these are always associated with an elongated streamer passing over the Iberian peninsula. A strong lee cyclogenesis effect then generates strong surface winds advecting moist Mediterranean air northward over the Alps. The present result would explain why streamers apparently have a stronger effect than vortices: the former have a larger radius of influence because they have a larger maximum length scale. HMR talk about the vertical penetration depth, but what is important here is the dramatic difference in the horizontal extent of the disturbance. The downward vertical penetration depth can never exceed the density-scale height in small–Rossby number flow, but we see here that the horizontal extent of the flow is not limited by the corresponding deformation radius.

Many quasigeostrophic and semigeostrophic studies use a rigid lid to represent the tropopause, following Eady (1949). This drastic approximation is tolerated because of the extreme simplification it brings to the dynamical system, especially when combined with the assumption of uniform potential vorticity in the troposphere. The theory of J94 shows how to relax the rigid-lid approximation while retaining much of the simplicity of the rigid-lid model. The rigid-lid approximation, for Boussinesq flow, can be obtained by taking the limit $N_s \to \infty$ in (23) and (25). The coefficients for the vertical displacement of the tropopause naturally vanish in this limit. The coefficients for the streamfunction are given by

$$\tilde{G}_1^{\theta|\text{lid}} = \frac{f}{\lambda H_{00} N_t} \coth(N_t \lambda H_{\text{tp}}/f), \tag{26a}$$

$$\tilde{G}_1^{u|\text{lid}} = \frac{f}{\lambda H_{00} N_t} \tanh(N_t \lambda H_{\text{tp}}/f). \tag{26b}$$

For large λ these differ from the free tropopause solutions by a factor $(N_s - N_t)/N_s$, which is about 0.6 here. At small λ the problem is more serious, with the ratio tending to λ and λ^{-1} for the lower boundary conditions on θ and u, respectively. Of course, the Boussinesq approximation is not, in any case, valid in this

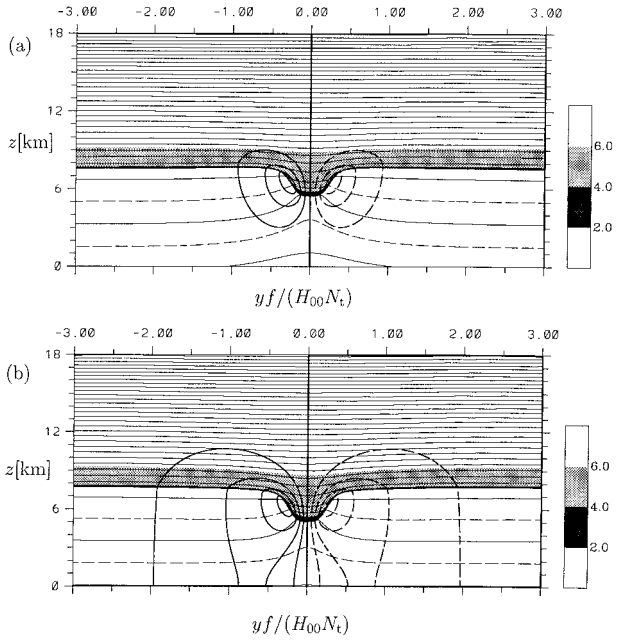

FIG. 4. Numerical solutions of Eq. (16), showing the full domain. Here $\theta_{sl} = 15$ K, $y_{sl} = 0.25$, $\theta_{in} = 2$ K, and $y_{in} = 0.125$. The lower boundary condition is (a) $u_{gr} = 0$ and (b) $\theta_{gr} = 0$. The thin solid lines are isentropes with an interval of 10 K; the thick lines are the wind with interval 5 m s^{-1}. Additional thin dashed contours mark $\theta = 305$ and 315 K. Potential vorticity values between 2 and 6 PVU are shaded, with darker shading between 2 and 4 PVU.

limit. Here $\tilde{G}_1^{\theta|\text{lid}}$ corresponds to the Eady edge wave investigated by Bishop (1993a,b).

5. Shear line structure

This section presents some primitive equation shear line structures. The dynamical system is defined by the potential vorticity equation [(13)] and Eqs. (12a) and (12b), relating the wind and temperature to the geopotential. The flow structure is specified through the functional relationship between θ and P [Eq. (15)] and the potential temperature at which the transition between the stratosphere and troposphere is made. When this information is complemented with appropriate boundary conditions and details of the transition at the tropopause [Eqs. (16), (17)], the solution is fully determined. The solution is not sensitive to the form of the transition defined in (16) provided it is sufficiently sharp.

Figure 4 shows the full domain and its reflection in the axis of symmetry at $y = 0$. General parameters are as given at the end of section 3; in addition, the strength of the tropopause potential temperature anomaly is $\theta_{sl} = 15$ K, the width of the shear line is $y_{sl} = 0.25$, and the sharpness of the edges of the shear line is defined by $y_{in} = 0.125$ (giving a smooth structure). The Rossby number (defined as the maximum wind speed divided by the y coordinate of this maximum times f) is then 0.816 for the zero wind lower boundary condition and 0.969 for the isentropic lower boundary condition. Shading shows the P structure, thin lines the isentropes, and thicker lines the velocity. As expected from QGT theory, the inversion with the lower boundary condition $u = 0$ at $z = 0$ decays rapidly at large $|y|$ whereas the other boundary condition creates a flow that extends out to the lateral boundaries. The structure is well isolated from the upper boundary in both cases.

The structure is clearer in Fig. 5, showing a close-up of the region $y = (0, 1.5)$ and $z = (0, 12)$ km. The vertical displacement of the dynamical tropopause is about 2–2.5 km. The flow has been defined by specifying the potential temperature of the tropopause, that is, the potential temperature at which the transition from tropospheric to stratospheric potential vorticity values is made. The height of the tropopause is determined by solving the differential equation that expresses the balance condition. This is similar to the procedure used by Hoskins and Bretherton (1972), except that here the position of the tropopause adjusts automatically as the potential temperature of the solution is updated, rather than being nudged into position by a separate algorithm. The potential temperature variations on the tropopause have their origins in the diabatically maintained equator-to-pole gradient. Vortices and shear lines are then generated when horizontal winds acting on this gradient create blobs and streamers. Since the flow is balanced, its structure can be evaluated without specific reference to these formation processes. In particular, the vertical displacement of the tropopause can be determined from the potential temperature of the tropopause and knowledge of the potential vorticity structure of the troposphere and stratosphere. In other words, it is not necessary to follow the vertical advection of the tropopause by the ageostrophic velocity explicitly. Indeed, that velocity can be derived diagnostically by differencing the tropopause height evaluated at two time instants.[1] A similar method, using the thermodynamic equation to evaluate the vertical velocity diagnostically, was used by Wirth et al. (1998) to evaluate the vertical velocity 500 m under the tropopause. They used the minimal model, which neglects non-Boussinesq effects and interactions with the lower boundary. In this idealization the vertical velocity of the tropopause in the QGT theory vanishes.

Figure 6 shows a close-up of the shear line at three grid resolutions. At the intermediate resolution there is a slight waviness in the potential vorticity contours.

[1] One reviewer suggested that δz_a calculated in J94 was not a real vertical displacement. In J94 it is, however, clearly and unambiguously defined as the vertical displacement of the tropopause. A theoretical relationship between the vertical displacement of the tropopause and potential temperature anomalies on the tropopause was derived for low Rossby number. The validity of the derivation is confirmed by comparison with numerical solutions of the primitive equations reported here.

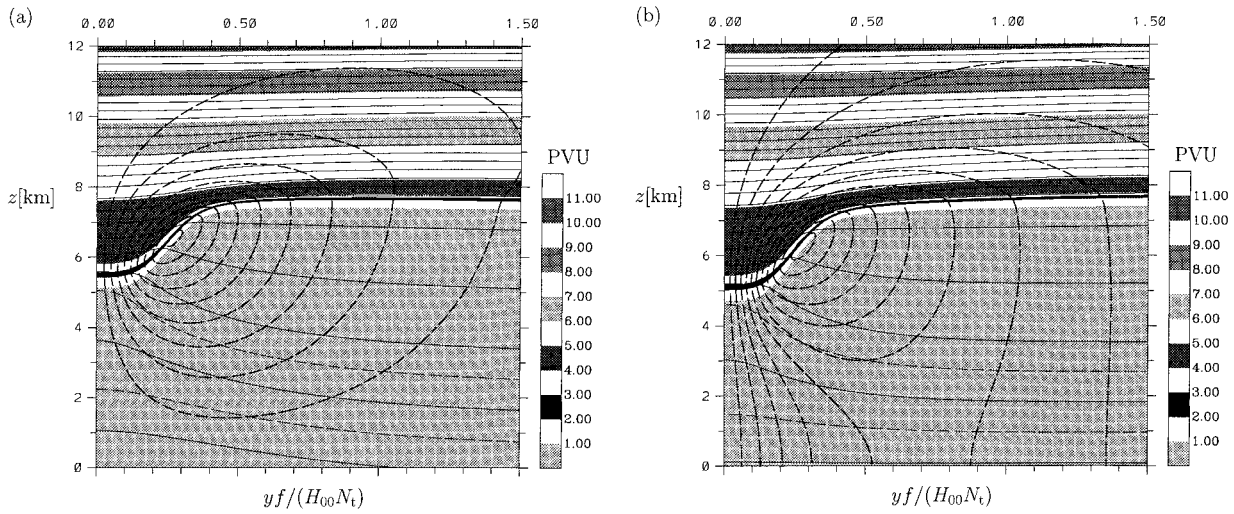

FIG. 5. As in Fig. 4 but showing a close-up of the region $y = (0, 1.5)$, $z = (0, 12)$. The contour intervals are 2 m s^{-1} and 5 K. The thin dashed lines mark $\theta = 302.5$ and 307.5 K. Shading of potential vorticity as indicated in the color bar in PVU.

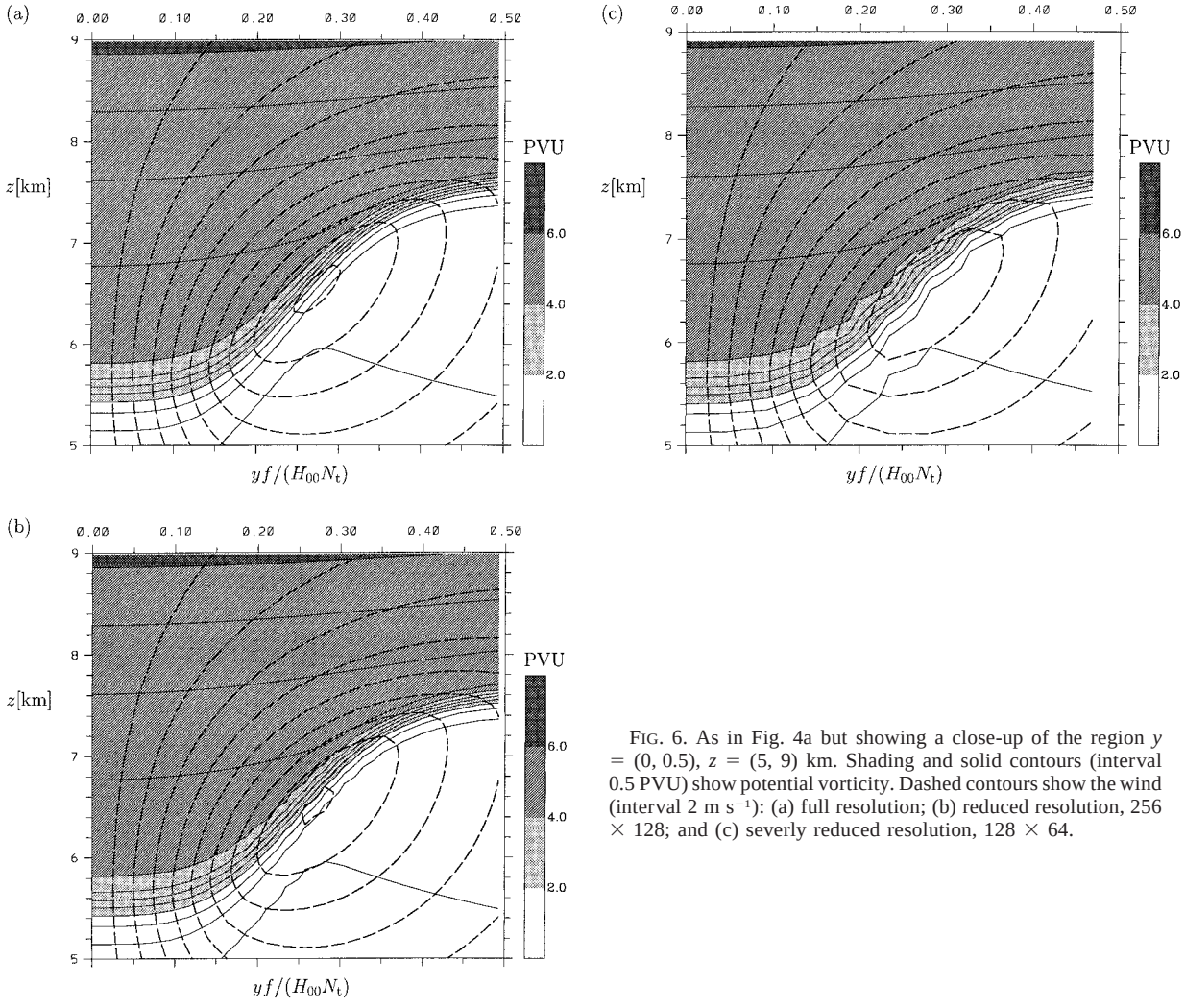

FIG. 6. As in Fig. 4a but showing a close-up of the region $y = (0, 0.5)$, $z = (5, 9)$ km. Shading and solid contours (interval 0.5 PVU) show potential vorticity. Dashed contours show the wind (interval 2 m s^{-1}): (a) full resolution; (b) reduced resolution, 256 $\times$ 128; and (c) severly reduced resolution, 128 $\times$ 64.

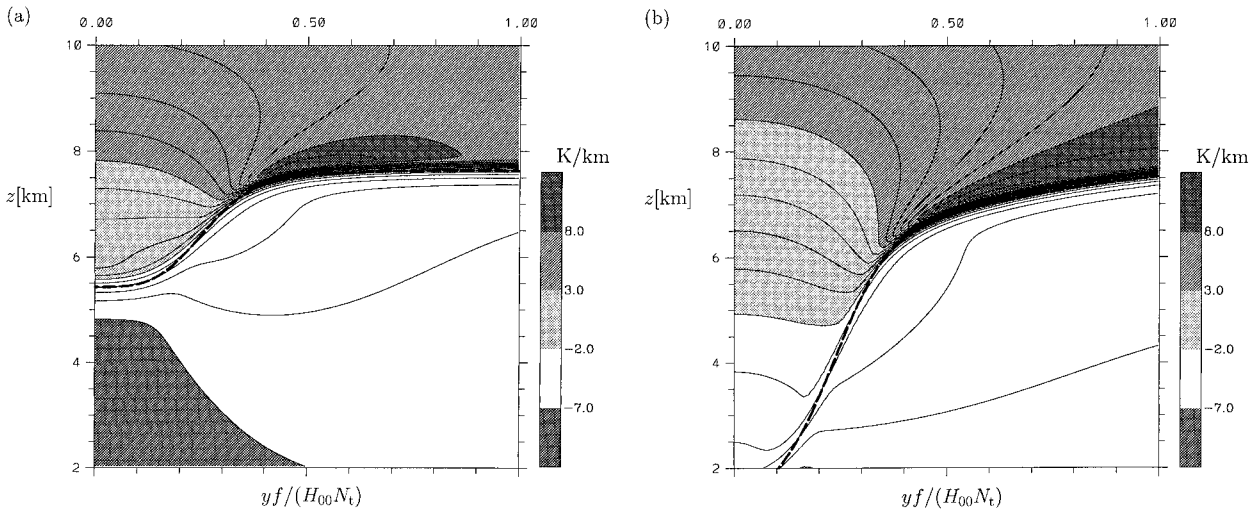

FIG. 7. The lapse rate (shading and solid contours, interval 1 K km^{-1}). The 2-PVU Ertel potential vorticity surface is shown by a thick dashed line. The shear lines shown are (a) as in Figs. 4a and 5a, and (b) $\theta_{gr} = 0$ and $\theta_{sl} = 25$ K.

When the resolution is reduced further, to one-quarter of the default resolution, this feature becomes more pronounced. These features are independent of all the numerical parameters except resolution; they occur because the grid cannot fully resolve the sharp gradients in potential vorticity at the tropopause. At the lowest resolution there are only 10 grid points spanning the region plotted. The maximum wind speed is, in order of decreasing resolution, 18.28, 18.18, and 17.87 m s^{-1}. The change caused by halving the resolution used in this study is minimal. We can thus conclude that the flow structure is well resolved at the higher resolution and that the basic structure of the isentropes and wind field is also well resolved at the intermediate resolution. The latter is, however, marred by noisiness in the potential vorticity field in the vicinity of the tropopause.

Figure 7 shows the lapse rate corresponding to the flow shown in Fig. 3a and also for a stronger shear line. In the latter there is a marked discrepancy between the position of the thermal tropopause and the dynamical tropopause. The former cuts through the potential vorticity anomaly. Both above and below the anomaly the lapse rate is reduced with respect to that in the corresponding undisturbed air mass. Within the anomaly the lapse rate is less than that of the undisturbed stratosphere but greater than that of the troposphere. There is a region of enhanced static stability in the stratosphere just outside the anomaly, at $y = 0.5$. This is associated with isentropes dipping into the anomaly.

The rest of this section looks at some other parameter values and compares the results with the predictions of the QGT theory described in section 3. The results are presented in the form of the vertical displacement of the tropopause (δz_a) and the horizontal wind evaluated on the tropopause [$u_{tp}(y) = u(y, H_{tp} + \delta z_a)$]. The vertical structure is in all cases qualitatively similar to that shown in the previous figures. The vertical displacement of the tropopause illustrates the extent to which the QGT theory can give a qualitative description of the ageostrophic motion of the tropopause, in so far as this displacement is a consequence of ageostrophic adjustment acting to maintain geostrophic balance.

Figure 8 compares the horizontal velocity on the tropopause and the vertical displacement of the tropopause found in the primitive equation model and those predicted by QGT theory. The Rossby number is about 0.13. This shows that the QGT theory does give the correct leading-order result as the Rossby number approaches zero. The results are shown for both lower boundary conditions. The relative errors are of the order 7% for the vertical displacement and slightly less for the wind field. Also shown are the various approximations to the full QGT theory. The Boussinesq approximation introduces an error of 15%–20%, overestimating both the vertical displacement and the strength of the wind. The minimal approximation, ignoring the lower boundary, lies between the Boussinesq curves for the two lower boundary conditions considered here.

The two lower curves in Fig. 8b indicate the results using the rigid-lid approximation. As a quantitive estimate this is clearly wrong, though the position of the jet and the length scale of the decay away from the jet are reasonable. Much of the discrepancy can be dealt with by simply rescaling by $(N_s - N_t)/N_s$. This will work so long as the dominant scales are somewhat less than the Rossby radius.

Figure 9 shows a range of stronger flows, increasing up to Rossby number 1.221. The errors in u_{tp} are as great, if not larger, at large distances from the shear line as they are within the shear line. This is somewhat surprising at first sight, since the Rossby number is largest within the shear line. It is a reminder that the problem is a nonlocal one. The QGT solution at large distances from the shear line is self-consistent, but it does not

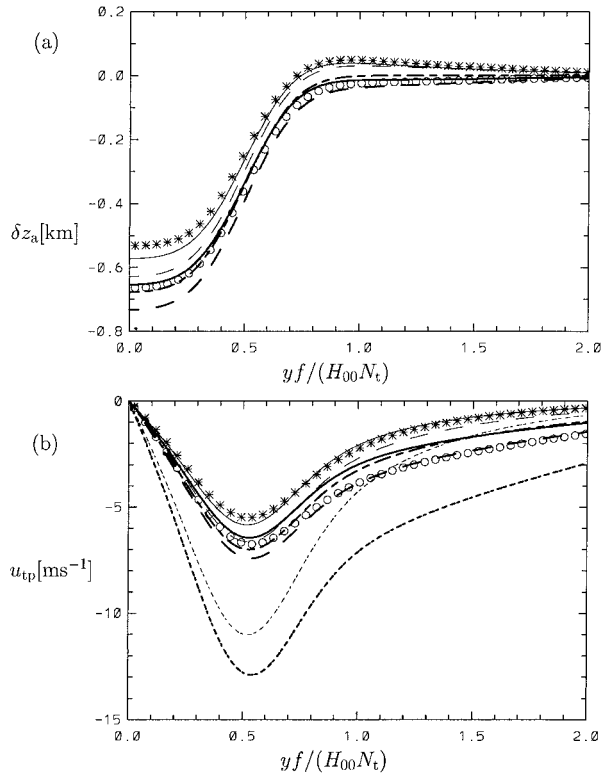

FIG. 8. Vertical displacement of the tropopause (a) and horizontal velocity on the tropopause (b) for a shear line with $y_{sl} = 0.5$, $\theta_{in} = 2$ K, $y_{in} = 0.25$, and shear line strength $\theta_{sl} = 5$ K. The corresponding Rossby number is about 0.13. The solid lines show the full quasigeostrophic solution for the two lower boundary conditions. The corresponding primitive equation solutions are shown in symbols. Dashed lines show the Boussinesq approximation, and alternating long and short dashes the minimal model. (b) The lower two lines correspond to the rigid-lid model. The lighter lines and stars correspond to the $u_{gr} = 0$ solution, the thicker lines and circles to $\theta_{gr} = 0$.

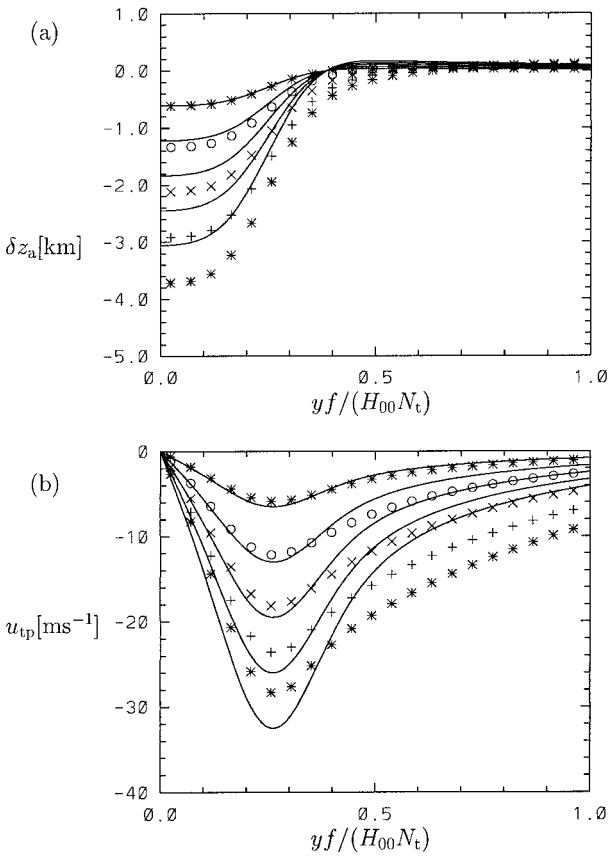

FIG. 9. Vertical displacement of the tropopause (a) and horizontal velocity on the tropopause (b). The lines show the quasigeostrophic inversion and the symbols show corresponding primitive equation results. Rossby numbers are 0.263, 0.546, 0.816, 1.061, and 1.221.

correctly match the strength of the potential vorticity anomaly that is generating it. This is related to an overestimate in the decay rate in the range $y \approx 0.3$–0.7. In QGT theory the inverse of the static stability is effectively estimated as

$$\left(\frac{\partial\theta_{sr}}{\partial z} + \frac{\partial\theta'}{\partial z}\right)^{-1} \approx \left(\frac{\partial\theta_{sr}}{\partial z}\right)^{-1}\left[1 - \frac{\partial\theta'}{\partial z}\left(\frac{\partial\theta_{sr}}{\partial z}\right)^{-1}\right].$$

When $\partial\theta'/\partial z$ approaches $d\theta_{sr}/dz$ this gives an overestimate of the static stability anomaly and, hence, an overestimate of the absolute vorticity anomaly (since the two must, under the assumption of uniform potential vorticity, balance each other).

Figure 10 shows shear lines similar to those in Fig. 9 but with the stratospheric static stability reduced by a third. The difference between Figs. 9 and 10 illustrates the tendency for the static stability in the stratosphere to reduce the vertical displacement and enhance the strength of the jet. That is, as N_s^2 is increased there is a smooth transition toward the rigid-lid model.

In conclusion, the QGT theory is correct in the limit of low Rossby number, despite the presence of large isentropic and isobaric gradients of N^2. This confirms the validity of the mathematical analysis in J94. The errors, however, become large at Rossby numbers of the order one-half. This is a severe limitation, though large-scale features with Rossby numbers in the range where the theory is quantitatively accurate (about 0.3 and less) do play a significant role in midlatitude dynamics.

6. Conclusions

The analysis of J94 is based on a model with a uniform value quasigeostrophic potential vorticity in the troposphere and a higher uniform value in the stratosphere. The analysis in section 2 has shown how this situation is related to the distribution of Ertel's potential vorticity. The constancy of q requires that the isentropic gradient of P vanish (Charney and Stern 1962). The new version of Charney and Stern's result, presented in section 2, clarifies the relation between these two important potential vortices.

A series of shear lines associated with a depressed tropopause have been constructed. The flows exhibit

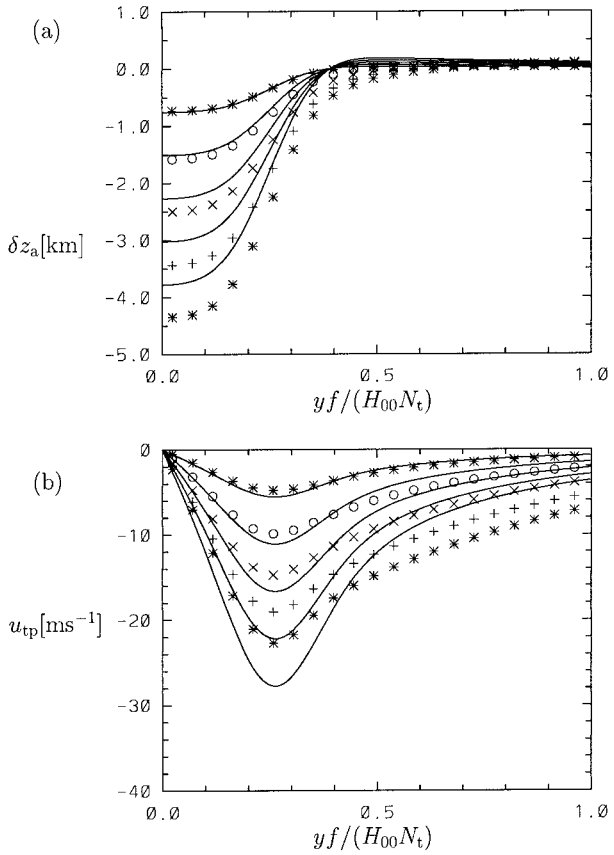

FIG. 10. As in Fig. 9 but with $\Gamma_s = 12$ K km^{-1}. Rossby numbers are 0.220, 0.453, 0.673, 0.869, and 1.034.

well-known features of cyclonic potential vorticity anomalies, with enhanced static stability inside the anomaly relative to the same isentropes outside the anomaly. The highest static stabilities occur in the anticyclonic shear in the stratosphere, just ouside the shear line. The lowest stabilities occur in the cyclonic shear immediately under the depressed tropopause. These features are associated with general properties of potential vorticity anomalies described by HMR.

The main intention of this paper was to evaluate the accuracy of QGT theory applied to shear lines in the upper troposphere generated by the intrusion of stratospheric air. For Rossby numbers up to 0.3 the theory gives a quantitatively accurate prediction of the geostrophic wind and ageostrophic vertical displacement of the tropopause associated with a prescribed potential temperature anomaly. At Rossby number of 0.6 there is still substantial agreement, but the errors are significant, with a substantial underestimate of u_{tp} outside the shear line (see Fig. 9b), for instance. The usefulness of the theory lies in the fact that it not only filters out gravity waves through the quasigeostrophic approximation, but also facilitates the reduction of the dynamical problem from three to two dimensions (in the present case, from two to one dimension). This reduction is achieved by assuming that the isentropic gradients of potential vorticity vanish except at the tropopause. Although the dimensionality of the evolution equations is thus reduced, the full three-dimensional structure is carried implicitly and can be recovered diagnostically.

The Boussinesq version of the QGT model is considerably more accurate than the rigid-lid model without incurring much extra complexity. Variations in tropopause height of several kilometers can be described by relatively simple formulas that relate them to tropopause potential temperature anomalies formed by quasi-horizontal advection. Just as in the vacuum cleaner anology of HMR, the vertical motion is implied from changes in the structure of the isentropes as they respond to the horizontal advection of potential vorticity. The vertical motion of the tropopause can be deduced from the change in its vertical displacement that must accompany quasi-horizontal advection of tropopause potential temperature anomalies.

The QGT theory thus provides a useful description of the relation between potential temperature, height, and geostrophic streamfunction of the tropopause for a small but significant range of Rossby numbers. The theory correctly indicates the changes in structure of an anomaly associated with a change in the lower boundary condition or a change in stratospheric stability. The theory gains its power from the fact that, in uniform potential vorticity flow, the vertical structure associated with individual components of a horizontal Fourier decomposition can be expressed analytically.

The inversion shows that when an upper anomaly becomes detached from a compensating surface anomaly, the horizontal extent of the winds that are generated is limited only by the largest length scale of the upper anomaly. If the lower boundary is neglected, on the other hand, the Rossby deformation radius provides an upper limit on the horizontal radius of influence. The difference arises from the interaction of an atmospheric anomaly in non-Boussinesq flow with the lower boundary. This means that a shear line passing over the Iberian peninsula, unlike a cutoff cyclone, is capable of generating a uniform southerly flow extending along the entire southern flank of the Alps, as observed by Massacand et al. (1998). Elongated streamers tend to have a larger scale, since the synoptic flow does not have enough energy to create axisymmetric vortices with comparable scales.

Acknowledgments. I would like to thank the anonymous reviewers and G. Zängl for helpful comments and corrections to an earlier manuscript.

APPENDIX

Various Asymptotic Limits

Some properties of the coefficients relating the streamfunction and vertical displacement to the poten-

tial temperature anomalies can be illuminated by studying the behavior of these coefficients in the limits of large and small wavenumber or distance. As noted in the text, the occurrence of several length scales in the problem does limit the usefulness of these results.

The limiting values of the streamfunction coefficient $\tilde{G}_1^u$ are given by

$$\tilde{G}_1^u(k, l) \to \tilde{G}_1^{\min}\left[1 + \frac{(N_s - N_t)}{2N_sN_t}\frac{f}{\lambda H_{00}}\right]^{-1}, \quad \lambda \to \infty; \tag{A1a}$$

$$\tilde{G}_1^u(k, l) \to \frac{[1 - \exp(-\varphi)](\Gamma_s - \Gamma_t)}{\Gamma_s} \times \left\{1 + \frac{2}{\varphi}\left[1 - \frac{\varphi}{\exp(\varphi) - 1}\right]\left(\frac{\lambda H_{00}N_t}{f}\right)^2\right\}^{-1}, \quad \lambda \to 0; \tag{A1b}$$

where $\varphi = H_{\text{tp}}/H_{00}$, the ratio of the tropopause height to the density-scale height.

For the zero potential temperature anomaly lower boundary condition we obtain

$$\tilde{G}_1^\theta(k, l) \approx \tilde{G}^u(k, l), \qquad \lambda \to \infty; \tag{A2a}$$

$$\tilde{G}_1^\theta(k, l) \to \frac{(\Gamma_s - \Gamma_t)f^2}{\Gamma_s H_{00}^2 N_t^2 \lambda^2[\exp(\varphi) - 1]}, \qquad \lambda \to 0. \tag{A2b}$$

The long-wave limit ($\lambda \to 0$) is analogous to the nondivergent vorticity equation, which would give $\psi \propto y$ at large distances and, hence, $u = constant$. In the present case this is prevented by the boundary conditions $u = 0$, so instead we see a linear trend $u \to 0$. In other words, the problem with this lower boundary condition cannot, in general, be made independent of the lateral boundaries (at least so long as attention is restricted to standard boundary conditions that specify ϕ and $\nabla\phi$: the physical boundary condition would involve specifying $\phi_{yy} = 0$ at the side boundaries, but it is not clear how this should be implemented numerically).

The Fourier transform of the coefficients $\tilde{G}_{1,2}$ gives the Green's function. The transform of the full expression has been evaluated numerically. The large y approximation obtained after some effort is

$$G_1^u(y) \approx \frac{2N_tH_{00}y^{-3/2}}{f(\sqrt{N_s^2 - N_t^2} + N_s\coth\chi)^2}\sqrt{\frac{N_sH_{00}}{\pi f}}\exp\left[\frac{-fy}{2N_sH_{00}}\right],$$

where $\chi = H_{\text{tp}}\sqrt{N_s^2 - N_t^2}/(2N_sH_{00})$. This form is obtained by considering the singularities of $\tilde{G}(0, l)$ in the complex l plane. The large y behavior is dominated by the singularity occuring nearest to the real axis, which is at $l = if(2N_sH_{00})$. This gives the scale of the exponential decay.

The near field is given by the transform of (A1a):

$$G_1^\theta(y) \approx G_1^u(y) \approx -\frac{(N_s - N_t)}{\pi N_s}\left\{\gamma + \ln\left[\frac{(N_s - N_t)}{N_sN_t}\frac{yf}{H_{00}}\right]\right\},$$

where $\gamma \approx 0.5772$ is Euler's constant. This transform has been evaluated by using

$$\int_{-\infty}^{\infty}\left(\frac{1}{1 + |s|} - \frac{1}{\sqrt{1 + s^2}}\right)e^{iys}\,ds \to -2\ln 2 + O(y^2)$$

and

$$\int_{-\infty}^{\infty}\frac{1}{\sqrt{1 + s^2}}e^{iys}\,ds = K_0(|y|) \to -\left(\gamma + \ln\frac{|y|}{2}\right) + O(y^2).$$

The first identity follows by taking a Taylor expansion of e^{iys}; the second can be found in Olver (1974).

REFERENCES

Andrews, D. G., J. R. Holton, and C. B. Leovy, 1987: *Middle Atmosphere Dynamics.* International Geophysics Series, Vol. 40, Academic Press, 489 pp.

Appenzeller, C., and H. C. Davies, 1992: Structure of stratospheric intrusions into the troposphere. *Nature,* **358,** 570–572.

——, ——, and W. A. Norton, 1996: Fragmentation of stratospheric intrusions. *J. Geophys. Res.,* **101,** 1435–1456.

Bayramli, A., and M. N. Juckes, 1998: The instability of upper tropospheric shear lines. *Atmos. Environ.,* **32,** 3113–3121.

Berrisford, P., J. C. Marshall, and A. A. White, 1993: Quasigeostrophic potential vorticity in isentropic coordinates. *J. Atmos. Sci.,* **50,** 778–782.

Bishop, C. H., 1993a: On the behaviour of baroclinic waves undergoing horizontal deformation. I: The '*RT*' phase diagram. *Quart. J. Roy. Meteor. Soc.,* **119,** 221–240.

——, 1993b: On the behaviour of baroclinic waves undergoing horizontal deformation. II: Error-bound amplification and Rossby wave diagnostics. *Quart. J. Roy. Meteor. Soc.,* **119,** 241–267.

——, and A. J. Thorpe, 1994: Potential vorticity and the electrostatic analogy: Quasi-geostrophic theory. *Quart. J. Roy. Meteor. Soc.,* **120,** 713–731.

Blumen, W., 1978: Uniform potential vorticity flow: Part I. Theory of wave interactions and two-dimensional turbulence. *J. Atmos. Sci.,* **35,** 774–783.

Browning, K. A., 1993: Evolution of a mesoscale upper tropospheric vorticity maximum and comma cloud from a cloud-free two-dimensional potential vorticity anomaly. *Quart. J. Roy. Meteor. Soc.,* **119,** 883–906.

Charney, J. G., and M. E. Stern, 1962: On the stability of internal baroclinic jets in a rotating atmosphere. *J. Atmos. Sci.,* **19,** 159–172.

Danielsen, E. F., 1968: Stratospheric-tropospheric exchange based on radioactivity, ozone and potential vorticity. *J. Atmos. Sci.,* **25,** 502–518.

Eady, E. T., 1949: Long waves and cyclone waves. *Tellus,* **1,** 33–52.

Held, I. M., R. T. Pierrehumbert, S. T. Garner, and K. L. Swanson, 1995: Surface quasi-geostrophic dynamics. *J. Fluid Mech.,* **282,** 1–20.

Holopainen, E. O., and L. Rontu, 1981: On shear lines in the upper troposphere over Europe. *Tellus,* **33,** 351–359.

Hoskins, B. J., and F. P. Bretherton, 1972: Atmospheric frontogenesis models: Mathematical formulation and solution. *J. Atmos. Sci.,* **29,** 11–37.

——, M. E. McIntyre, and A. W. Robertson, 1985: On the use and significance of isentropic potential vorticity maps. *Quart. J. Roy. Meteor. Soc.,* **111,** 877–946.

Juckes, M. N., 1994: Quasigeostrophic dynamics of the tropopause. *J. Atmos. Sci.,* **51,** 2756–2768.

——, 1995: Instability of surface and upper-tropospheric shear lines. *J. Atmos. Sci.,* **52,** 3247–3262.

——, 1997: The mass flux across the tropopause: Quasi-geostrophic theory. *Quart. J. Roy. Meteor. Soc.,* **123,** 71–99.

Kleinschmidt, E., Jr., 1950: Über Aufbau und Entstehung von Zyklonen. *Meteor. Rundsch.,* **3,** 1–6.

Lait, L. R., 1994: An alternative form for potential vorticity. *J. Atmos. Sci.,* **51,** 1754–1759.

Massacand, A. C., H. Wernli, and H. C. Davies, 1998: Heavy precipitation on the Alpine southside: An upper-level precursor. *Geophys. Res. Lett.,* **25,** 1435–1438.

Olver, F. W. J., 1974: *Introduction to Asymptotics and Special Functions.* Academic Press, 297 pp.

Reed, R. J., 1955: A study of a characteristic type of upper-level frontogenesis. *J. Meteor.,* **12,** 226–237.

Sadourny, R., 1985: Quasi-geostrophic turbulence: An introduction. *Turbulence and Predictability in Geophysical Fluid Dynamics and Climate Dynamics,* M. Ghil, Ed., Elsevier Science, 133–158.

Salby, M. L., and M. N. Juckes, 1994: An algorithm for retrieving the motion field from satellite measurements of tracer behavior. *J. Geophys. Res.,* **99,** 1403–1418.

Thorpe, A. J., and C. H. Bishop, 1995: Potential vorticity and the electrostatics analogy: Ertel-Rossby formulation. *Quart. J. Roy. Meteor. Soc.,* **121,** 1477–1495.

Vallis, G. K., 1996: Potential vorticity inversion and balanced equations of motion for rotating and stratified flows. *Quart. J. Roy. Meteor. Soc.,* **122,** 291–322.

Wirth, V., 1995: Diabatic heating in an axisymmetric cut-off cyclone and related stratosphere-troposphere exchange. *Quart. J. Roy. Meteor. Soc.,* **121,** 127–147.

——, C. Appenzeller, and M. N. Juckes, 1997: Signatures of induced vertical air motion accompanying quasi-horizontal roll-up of stratospheric intrusions. *Mon. Wea. Rev.,* **125,** 2504–2519.